UNIVERSITY OF LEEDS

Article:
Zhuang, PZ orcid.org/0000-0002-7377-7297 and Yu, HS orcid.org/0000-0003-3330-1531 (2019) Two-dimensional elastoplastic analysis of cylindrical cavity problems in Tresca materials. International Journal for Numerical and Analytical Methods in Geomechanics, 43 (8). pp. 1612-1633. ISSN 0363-9061

https://doi.org/10.1002/nag.2925

Two-dimensional elastoplastic analysis of cylindrical cavity problems in Tresca materials

Pei-Zhi Zhuang*, Hai-Sui Yu

School of Civil Engineering, Faculty of Engineering, University of Leeds, LS2 9JT Leeds, UK

***Corresponding Author, Email: P.Zhuang@leeds.ac.uk

ABSTRACT:

This paper presents analytical elastic-plastic solutions for static stress loading analysis and quasi-static expansion analysis of a cylindrical cavity in Tresca materials, considering biaxial far-field stresses and shear stresses along the inner cavity wall. The two-dimensional static stress solution is obtained by assuming that the plastic zone is statically determinate and using the complex variable theory in the elastic analysis. A rigorous conformal mapping function is constructed, which predicts that the elastic-plastic boundary is in an elliptic shape under biaxial in-situ stresses and the range of the plastic zone extends with increasing internal shear stresses. The major axis of the elliptical elastic-plastic boundary coincides with the direction of the maximum far-field compression stress. Furthermore, considering the internal shear stresses, an analytical large-strain displacement solution is derived for continuous cavity expansion analysis in a hydrostatic initial stress filed. Based on the derived analytical stress and displacement solutions, the influence of the internal shear stresses on the quasi-static cavity expansion process is studied. It is shown that additional shear stresses could reduce the required normal expansion pressure to a certain degree, which partly explains the great reduction of the axial soil resistance due to rotations in rotating cone penetration tests. In addition, through additionally considering the potential influences of biaxial in-situ stresses and shear stresses generated around the borehole during drillings, an improved cavity expansion approach for estimating the maximum allowable mud pressure of horizontal directional drillings (HDDs) in undrained clays is proposed and validated.

Keywords: cavity expansion, conformal mapping function, shear stress, biaxial in-situ stresses, rotating cone penetration test, horizontal directional drilling

1 | INTRODUCTION

Cavity expansion theory has been extensively applied in various fields of geotechnical engineering such as interpretation of cone penetration tests (CPTs), prediction of soil resistance experienced by plate anchors and piles, stability analysis of tunnels and boreholes (e.g. blow out failure associated with loading and local collapse associated with unloading) [1-6]. These successful applications greatly stimulated the development of analytical cavity expansion solutions over the past decades. It is noted that analytical elastic-plastic solutions, in general, have been derived by assuming that the cavity is uniformly loaded by increasing internal normal pressures in a hydrostatic initial stress field. In reality, however, the in-situ soil stresses are not uniform in most cases, and the horizontal earth pressure at rest is often expressed as K_0 times of that in the vertical direction instead (i.e. $\sigma_{h0} = K_0\sigma_{v0}$) [7, 8]. Meanwhile, a great amount of shear stress might be applied or generated around the inner cavity wall in the process of rotary drilling/excavation, accommodation of screw piles or rotating penetration tests [9-13]. It has been reported that the biaxial in-situ stresses (K_0 effect) and internal shear stresses need to be additionally taken into account for further improving the accuracy of the cavity expansion theory in many applications [13-16], for example, in estimating the tip resistance of rotating CPTs and predicting the maximum mud pressure of HDDs, in particular, at relatively shallow depths [17-19]. To account for the additional influences of these two factors during loading/expansion of a cylindrical cavity in undrained clays, both static stress analysis and quasi-static expansion analysis adopting the linear elastic-perfectly-plastic Tresca model are carried out in this paper.

The stress field developed around a cavity primarily depends on the material strength and imposed boundary conditions. For a cavity with axisymmetric geometry and stress conditions, the stress analysis usually can be simplified to a one-dimensional equilibrium problem, which facilitated the development of a number of analytical elastic and elastic-plastic solutions [1]. When non-axisymmetric geometry and/or stress boundary conditions are considered, more advanced mathematical techniques such as the complex variable theory [20, 21], perturbation methods [22, 23], variational approaches [24] and numerical techniques [25, 26] tend to be required. Among these methods, the complex variable theory in conjunction with the conformal mapping technique provides a very powerful analytical tool for the elastic analysis

around a cavity with various boundary conditions [20, 27]. This method has also been extended to the analysis of a cylindrical cavity surrounded by strain-hardening materials obeying the power-law [28, 29]. However, these methods cannot be directly applied to the analysis in materials characterised by elastic-perfectly plastic models since the difference between elastic and plastic constitutive equations. To address this problem, Galin [30] creatively proposed an analytical approach for the analysis of a circular cavity embedded in an infinite plate under biaxial remote stretching loadings. By assuming that the plastic zone is statically determinate and using the complex variable theory in the elastic analysis, both constant and polynomial types of far-field stresses were studied by Galin [30]. Although minor mistakes existed in these solutions as found and improved by Ochensberger, et al. [31] and Tokar [32] respectively, it is generally believed that this methodology greatly facilitated the development of analytical/semi-analytical solutions for the two-dimensional elastic-plastic analysis of a series of problems with similar boundary conditions [33-38].

Comparing with the problem of Galin [30], uniform shear stresses at the inner cavity wall are additionally considered in this study. As a consequence, Galin's [30] approach to establishing the conformal mapping function cannot be applied to deal with this problem since the plastic state is no longer biharmonic [37]. Although Parasyuk [37] has given the form of the conformal mapping function for this problem (see Appendix B) based on Harnack's theorem, the mapping function has not been completely determined. Consequently, the range of the plastic zone is not known, and the elastic field cannot be obtained. In order to give a complete solution to this problem, the conformal mapping function is further explored by introducing Laurent decomposition theorem in the analysis of stress continuity conditions across the elastic-plastic boundary, and closed-form Kolosov-Muskhelishvili complex potentials [20] for the elastic analysis are then derived by using a Fourier series and the Cauchy integral method in this paper. This analytical stress solution is validated by comparing with the finite element method and Galin's [30] solution.

To further demonstrate the necessity and importance of considering the internal shear stresses and/or biaxial in-situ stresses in practical geotechnical problems, the newly derived static stress solution and

quasi-static expansion solution are applied to estimate the normal soil resistance experienced by a vertically advancing cone with rotations and predict the maximum mud pressure during HDDs:

(1) The axial penetration resistance could be significantly reduced by rotations [9, 18, 19]. Therefore, rotating a pushing cone penetrometer is regarded as one of the most feasible physical methods to eliminate the interface friction in modelling the root tip-soil interaction (lubricated interface due to the sloughing off of border cells and mucilage from roots) [9, 11, 18]. In rotating CPTs, shear stresses would be generated around the sliding interface, which not only decrease the frictional resistance both on the cone tip and the shaft and may also lead to additional plastic failure in the surrounding soil [18, 19]. The reduction of the axial tip resistance is usually attributed to the reorientation of the frictional resistance at the cone and the additional plastic deformation caused by the generated shear stresses [18, 19]. The former effect has been explained by Bengough, et al. [18] based on quasi-static equilibrium analysis. Unfortunately, analytical methods accounting for the latter effect are still rarely available. According to the analogy of cone penetration and continuous expansion of a cylindrical cavity [39, 40], an analytical quasi-static expansion solution is developed to capture the additional influences of cone rotations on the normal soil resistance in this paper.

(2) HDD becomes a popular alternative to traditional open-cut excavation for pipeline and underground utility conduit installation due to its higher flexibility in operation and potential economic and environmental benefits [41-43]. During HDDs, it requires continuous circulation of pressurized fluid in the bore to remove the cutting out, stabilize the bore formation, cool and clean the drill bit, and lubricate the pipe during installation. To avoid inadvertent drilling fluid returns and also effectively return the soil cutting from the boring path to the ground surface, the determination or control of the applied drilling fluid pressure remains a serious concern in the design and implementation of HDDs, especially the maximum allowable mud pressure [44-46]. Cylindrical cavity expansion solutions provide one of the most commonly used theoretical methods for estimating the maximum mud pressure during HDDs [5, 17, 42, 47], for example, the Delft cylindrical cavity expansion model (Delft solution) proposed by Luger and Hergarden [48] by extending Vesic's solution [49]. In the Delft solution, the in-situ stress field is simplified to be hydrostatic [5, 47]. However, for HDD practices implemented at relatively shallow depths, it has been

reported that the K_0 effect may exert significant influences on the maximum allowable mud pressure [17, 50]. Considering the K_0 effect, Xia and Moore [17] proposed an approximate method by replacing the elastic stresses in the Delft solution with Kirsch equations (i.e. m=0 in Appendix A) while estimating the maximum mud pressure in undrained clays. However, the elastic and plastic stresses were derived independently in their solution, and the elastic-plastic boundary was assumed to be circular regardless of the biaxial in-situ stresses. By using the more rigorous stress solution derived in this paper, the method of accounting for the K_0 effect is further improved. Meanwhile, the shear stresses potentially generated during pilot hole boring and reaming of HDDs are also considered in the new method.

2 | PROBLEM DEFINITION

A sufficiently large and thick soil medium (in comparison with the cavity size) with an inside cylindrical cavity is considered. As depicted in Figure 1, biaxial initial stresses apply at infinity, and uniform shear stresses act on the inner cavity wall. The surrounding medium is loaded monotonically by normal compression pressures on the inner cavity wall to the value of p_{in} with a sufficiently slow speed. The stress and deformation analysis are conducted under the assumption of plane strain. For convenience, both Cartesian coordinates (x, y, z) and cylindrical polar coordinates (r, θ, z) with the same origin at the centre of the cavity are utilised. It is worth noting that the defined remote stress conditions are sufficiently general because we always can set a coordinate system with axes parallel to the directions of the principal stresses at infinity. Within the cylindrical polar coordinates, the stress equilibrium equations in the radial and circumferential directions, respectively, are

$$\frac{\partial \sigma_{\mathrm{r}}}{\partial \mathrm{r}}+\frac{1}{\mathrm{r}} \frac{\partial \tau_{\mathrm{r}\theta}}{\partial \theta}+\frac{\sigma_{\mathrm{r}}-\sigma_{\theta}}{\mathrm{r}}=0 \tag{1}$$

$$\frac{1}{\mathrm{r}} \frac{\partial \sigma_{\theta}}{\partial \theta}+\frac{\partial \tau_{\mathrm{r}\theta}}{\partial \mathrm{r}}+\frac{2 \tau_{\mathrm{r}\theta}}{\mathrm{r}}=0 \tag{2}$$

where σ_{r}, σ_{θ} and $\tau_{\mathrm{r}\theta}$ are the radial, circumferential and shear stress components, respectively.

Taking tension as positive for normal stresses and rotation in the anticlockwise direction to the object as positive for shear stresses, the stress boundary conditions can be expressed as

105 $\sigma_r|_{r=R} = -p_{in}$, $\tau_{r\theta}|_{r=R} = mk$ $(-1 \le m \le 1)$ (3)

106 $P_\infty = (\sigma_y|_{y\to\infty} + \sigma_x|_{x\to\infty})/2 = -(\sigma_{v0} + \sigma_{h0})/2$, $\tau_\infty = (\sigma_y|_{y\to\infty} - \sigma_x|_{x\to\infty})/2 = (\sigma_{h0} - \sigma_{v0})/2$ (4)

107 where k is the yield stress under pure shear loading. m gives the relationship between k and the
108 internal shear stress.

109 The surrounding material is regarded as homogenous and isotropic, and it is characterised with an
110 elastic-perfectly plastic model. Specifically, the elastic response is described by Hooke's law until the
111 onset of yielding which obeys the Tresca yield criterion (i.e. Equation 5).

112 $(\sigma_r - \sigma_\theta)^2 + 4\tau_{r\theta}{}^2 = 4k^2$ (5)

113 # 3 | STATIC STRESS ANALYSIS

114 ## 3.1 | Plastic region

115 As an extension of Galin's [30] solution, this solution aims to provide an analytical method for the static
116 stress analysis of the soil around a cavity under conditions of: (a) the inner cavity is fully enclosed by a
117 connected plastic region, and the plastic stress field is statically determinate, (b) the plastic zone is
118 developed under monotonic loading, and no elastic unloading occurs in any case, and (c) the out-of-
119 plane stress component σ_{zz} always remains as the intermediate principal stress regardless of other
120 stresses [33, 35].

121 The static determinacy of the plastic field determines that the plastic stress field entirely depends on the
122 inner boundary conditions [35, 51]. Therefore, according to the axisymmetric fact of the geometry and stress
123 boundaries at the inner cavity wall, it is reasonable to assume

124 $\frac{\partial \sigma_r^p}{\partial \theta} = 0$, $\frac{\partial \sigma_\theta^p}{\partial \theta} = 0$, $\frac{\partial \tau_{r\theta}^p}{\partial \theta} = 0$ (6)

125 where the superscripts ^{e} and ^{p} indicate the stress components in the elastic and plastic region respectively.

126 The plastic stresses under loading can be obtained by solving the stress equilibrium equation (i.e.
127 Equation 3) and the yield criterion (i.e. Equation 5) with the given stress boundaries (i.e. Equation 3),
128 which are known as the Mikhlin's solution [13, 37] (i.e. Equations 7-9).

129 $$\sigma_r^p = k\left\langle \ln\left[\frac{(r/R)^2+\sqrt{(r/R)^4-m^2}}{1+\sqrt{1-m^2}}\right]-\sqrt{1-m^2(\frac{R}{r})^4}+\sqrt{1-m^2}\right\rangle - p_{in} \quad (7)$$

130 $$\sigma_\theta^p = k\left\langle \ln\left[\frac{(r/R)^2+\sqrt{(r/R)^4-m^2}}{1+\sqrt{1-m^2}}\right]+\sqrt{1-m^2(\frac{R}{r})^4}+\sqrt{1-m^2}\right\rangle - p_{in} \quad (8)$$

131 $$\tau_{r\theta}^p = mk\frac{R^2}{r^2} \quad (9)$$

132 **3.2 | Determination of conformal mapping function**

133 The elastic-plastic interface gives the outer boundary of the plastic zone and simultaneously provides
134 the inner boundary for computing the elastic stress field, which is, therefore, of great importance for
135 determining the range of the developed plastic zone and deriving the elastic stresses. The location of
136 the elastic-plastic boundary is generally determined by analysing the continuity conditions of the elastic
137 and plastic stresses across the interface. However, under non-equal far-field stresses, the elastic stress
138 field cannot be obtained prior to knowing its inner boundary conditions, namely the location of the
139 elastic-plastic boundary and stresses acting on it [30, 33, 35, 37]. Therefore, the elastic-plastic boundary is
140 described by a general form of the conformal mapping function first (i.e. Equation B1), and the elastic
141 stresses are represented in terms of general forms of Kolosov-Muskhelishvili complex potentials, $\Phi(\zeta)$
142 and $\Psi(\zeta)$ [20]. Based on the stress continuity conditions across the elastic-plastic boundary and the far-
143 field stress boundary conditions, the boundary values of $\Phi(\zeta)$ and $\Psi(\zeta)$ can be expressed as

144 $$\Phi(\zeta)+\overline{\Phi(\zeta)} = \frac{(\sigma_r^e+\sigma_\theta^e)}{2} = \begin{cases} k\left\langle \ln\left[\frac{\omega(\sigma)\overline{\omega(\sigma)}/R^2+\sqrt{[\omega(\sigma)\overline{\omega(\sigma)}]^2/R^4-m^2}}{1+\sqrt{1-m^2}}\right]+\sqrt{1-m^2}\right\rangle - p_{in} & ,\text{at } \gamma \quad (a) \\ P_\infty & ,\zeta\to\infty \quad (b) \end{cases} \quad (10)$$

145 $$\frac{\overline{\omega(\zeta)}}{\omega'(\zeta)}\Phi'(\zeta)+\Psi(\zeta) = \frac{(\sigma_\theta^e-\sigma_r^e+2i\tau_{r\theta}^e)}{2}e^{-2i\theta} = \begin{cases} k\left\langle \frac{\sqrt{[\omega(\sigma)\overline{\omega(\sigma)}]^2-m^2R^4}+mR^2i}{\omega(\sigma)\overline{\omega(\sigma)}}\right\rangle\frac{\overline{\omega(\sigma)}}{\omega(\sigma)} & ,\text{at } \gamma \quad (a) \\ \tau_\infty & ,\zeta\to\infty \quad (b) \end{cases} \quad (11)$$

where $\mathrm{i}=\sqrt{-1}$. γ represents the unit contour in the phase plane, corresponding to the elastic-plastic boundary. σ is the unit complex variable, which describes points on γ. $\sigma=\cos\phi+\mathrm{i}\sin\phi=\mathrm{e}^{\mathrm{i}\phi}$. and $\bar{\sigma}=1/\sigma$. ϕ is the argument of σ. The function of $\omega(\zeta)$ conformally maps the exterior of the elastic-plastic boundary in the physical plane onto the exterior region of the unit circle in the phase plane; $\overline{\omega(\zeta)}$ is its conjugate function. $\zeta=\xi+\mathrm{i}\eta=\rho\mathrm{e}^{\mathrm{i}\phi}$. ξ and η are the real and imaginary part of the complex variable ζ, respectively. ρ is the modulus of ζ. Boundary conditions of Equation 10b and Equation 11b specified the behaviour of the complex potentials at infinity as

$$\Phi(\infty)=\frac{\mathrm{P}_\infty}{2}+\mathrm{O}(\zeta^{-2}) \quad , \quad \Psi(\infty)=\tau_\infty+\mathrm{O}(\zeta^{-2}) \tag{12}$$

Owing to the additional consideration of the internal shear stresses, the plastic state is no longer biharmonic. Thus the mapping function cannot be determined by constructing a unified biharmonic stress function crossing the elastic-plastic interface as proposed by Galin [30]. Instead, Equations 10 and 11 are analysed based on Harnack's theorem. With this method, the form of the mapping function (i.e. Equation 13) was derived by Parasyuk [37], and a more general derivation is presented in Appendix B.

$$\omega(\zeta)=\alpha(\zeta+\frac{\beta}{\zeta}) \tag{13}$$

where $\beta=\tau_\infty/\mathrm{k}$.

Equation 13 gives that the elastic-plastic boundary is in an elliptic shape while $\beta\neq 0$, whose major axis is along the direction of the maximum far-field compression pressure under loading. However, the parameter α in Equation 13 has not been determined so far. Consequently, the range of the plastic zone and elastic stresses cannot be analytically obtained. To derive a complete solution to this problem, Equations 10 and 11 are further analysed as follows.

As the far-field stress conditions bound the behaviour of the right-hand side of Equation 10a at infinity [27, 52], the continuity condition of the mean stress can be re-expressed as

$$\Phi(\sigma)+\overline{\Phi(\sigma)}=\mathrm{k}\ln[\mathrm{F}(\sigma,\bar{\sigma})]+\mathrm{k}\sqrt{1-\mathrm{m}^2}-\mathrm{p}_{\mathrm{in}} \tag{14}$$

where $F(\sigma,\bar{\sigma})=\left\{\dfrac{\omega(\sigma)\overline{\omega(\sigma)}/R^2+\sqrt{[\omega(\sigma)\overline{\omega(\sigma)}]^2/R^4-m^2}}{(1+\sqrt{1-m^2})\sigma\bar{\sigma}}\right\}=\dfrac{f(\sigma)}{\sigma}\dfrac{\bar{f}(\bar{\sigma})}{\sigma^{-1}}$.

An elliptic elastic-plastic boundary is predicted by Equation 13, which is a closed smooth contour in the physical plane. $\ln[F(\sigma,\bar{\sigma})]$ in Equation 14 continues analytically on both sides of γ in an annulus of $0\le|\zeta-\sigma|\le\infty$. Thus, based on Laurent decomposition theorem [53], $\ln[F(\sigma,\bar{\sigma})]$ can be decomposed as a sum of two mutually conjugate functions, $d(\zeta)$ and $\bar{d}(\zeta^{-1})$, which are analytic in Ω^+ ($|\zeta|<1$) and Ω^- ($|\zeta|>1$) respectively. Then by multiplying $\dfrac{1}{2\pi i}\dfrac{d\sigma}{\sigma-\zeta}$ on both sides of Equation 14 and integrating it along γ, we obtain

$$F^+(\zeta)=\bar{d}(\zeta^{-1})-\overline{\Phi(\zeta)} \tag{15 a}$$

$$F^-(\zeta)=\Phi(\zeta)-d(\zeta)-(k\sqrt{1-m^2}-p_{in}) \tag{15 b}$$

where $d(\zeta)=k\ln[f(\zeta)/\zeta]$ and $\bar{d}(\zeta^{-1})=k\ln[f(\bar{\zeta})/\zeta^{-1}]$. $F^+(\zeta)$ and $F^-(\zeta)$ are analytic everywhere within the region of Ω^+ and Ω^-, respectively. Now the continuity condition of the mean stress across the unit circle γ can be expressed as $F^+(\sigma)=F^-(\sigma)$. Based on Liouville's theorem, which states $F^+(\zeta)$ and $F^-(\zeta)$ are identically equal to one and same constant due to the complex potentials are bounded at infinity. The boundary values of $d(\zeta)$ and $\bar{d}(\zeta^{-1})$ are studied in the extended complex plane with the form defined in Equation 14. By analysing Equation 14, it is obtained that

$$-\frac{P_\infty}{2}+\frac{1}{2}k\ln[\frac{2\alpha^2/R^2}{1+\sqrt{1-m^2}}]=\frac{P_\infty}{2}-\frac{1}{2}k\ln(\frac{2\alpha^2/R^2}{1+\sqrt{1-m^2}})-k\sqrt{1-m^2}+p_{in} \tag{16}$$

As a result, the undetermined parameter α in Equation 13 is obtained as

$$\alpha=\delta R e^{\frac{1}{2k}[p_{in}+P_\infty-k\sqrt{1-m^2}]} \quad (\text{with } \delta=\left[(1+\sqrt{1-m^2})/2\right]^{1/2}) \tag{17}$$

By now the conformal mapping function is completely determined. A new parameter δ is involved due to the additional consideration of the internal shear stresses comparing with Galin's [30] mapping

function. Equation 17 indicates that the size of the plastic region monotonically expands with an increasing expansion pressure. The lengths of the semi-major axis and the semi-minor axis of the elliptic elastic-plastic boundary can be expressed as $a_{ep} = \alpha(1+|\beta|)$ and $b_{ep} = \alpha(1-|\beta|)$ respectively. It is shown that the axis ratio (a_{ep} / b_{ep}) and axes directions of the elastic-plastic boundary entirely depend on the non-uniformity of far-field stresses (represented by the non-dimensional factor of β).

3.3 | Elastic stress analysis

The derived elastic-plastic boundary and plastic stresses provide the inner geometry and stress boundaries for the analysis of the outside elastic field. In other words, now the elastic field is equivalent to the problem that an elliptic cavity embedded in an infinite plane subjecting to non-uniform stresses at the inner cavity wall and biaxial stresses at infinity. At first, the elastic stresses are represented by the general forms of the elastic complex potentials (i.e. Equations 18 and 19) according to the complex potential method proposed by Muskhelishvili [20].

$$\Phi(\zeta) = \Gamma - \frac{X + iY}{2\pi(1+\chi)} \frac{1}{\zeta} + \Phi_0(\zeta) \tag{18}$$

$$\Psi(\zeta) = \Gamma' + \frac{\chi(X - iY)}{2\pi(1+\chi)} \frac{1}{\zeta} + \Psi_0(\zeta) \tag{19}$$

where $\Phi_0(\zeta) = \sum_{n=1}^{\infty} \frac{a_n}{\zeta^{n+1}}$, $\Psi_0(\zeta) = \sum_{n=1}^{\infty} \frac{b_n}{\zeta^{n+1}}$, which are holomorphic in the whole elastic region. $\Gamma = P_\infty / 2$ and $\Gamma' = \tau_\infty$, which describe the stress conditions at infinity. X and Y are components of the resultant vector of forces acting on the elastic-plastic boundary. $\chi = 3 - 4\nu$ for the plane strain problem. ν is Poisson's ratio.

The complex potentials are first sought with the assumption that both the stress and displacement components remain bounded at infinity, which implies that the resultant stresses vanish at infinity [20]. Mathematically, it requires $\Gamma = \Gamma' = 0$ and $X = Y = 0$. In this case, the complex potentials remain holomorphic in the outside region of contour γ. $\Phi_0(\zeta)$ and $\Psi_0(\zeta)$ fully satisfy the above requirements. According to the stress boundary conditions at the elastic-plastic boundary given in

213 Equations 10 and 11, it is not easy to derive the elastic complex potentials directly with simple algebraic
214 transformations, if possible. Alternatively, the inner stress boundaries of the mean stress (i.e. Equation
215 10a) are transformed into a Fourier series form as

$$\Phi_0(\sigma)+\overline{\Phi_0(\sigma)}=k\ln\left[\frac{(x_{ep}{}^2+y_{ep}{}^2)/R^2+\sqrt{(x_{ep}{}^2+y_{ep}{}^2)^2/R^4-m^2}}{1+\sqrt{1-m^2}}\right]+k\sqrt{1-m^2}-p_{in}-P_\infty$$
216 $$=G(\phi)=\sum_{-\infty}^{+\infty}A_n e^{in\phi}=\sum_{-\infty}^{+\infty}A_n\sigma^n \qquad (20)$$

217 where $A_n=\frac{1}{2\pi}\int_0^{2\pi}G(\phi)e^{-in\phi}d\phi$. $x_{ep}=\alpha(1+\beta)\cos\phi$ and $y_{ep}=\alpha(1-\beta)\sin\phi$.

218 In Equation 20, an even function of $G(\phi)$ is formed, which is a continuous real function in terms of the
219 argument ϕ within the interval of $0\le\phi\le 2\pi$. It means that $A_n = A_{-n}$ (real numbers) and coefficients
220 of the odd terms in $\Phi_0(\sigma)$ are infinitesimal. As $A_{-n}=\overline{A}_n$ and $\overline{\sigma}=\sigma^{-1}$, naturally both sides of Equation
221 20 can be split into two mutually conjugate parts. As a result,

222 $$\Phi_0(\sigma)=A_0/2+\sum_{n=1}^{+\infty}A_{-2n}/\sigma^{2n} \qquad (21)$$

223 As A_0 is vanishingly small, the requirement of $\Phi_0(\sigma)$ at infinity, namely $\Phi_0(\infty)=O(\zeta^{-2})$, is fulfilled.
224 More strictly in the mathematical formulation, the term with coefficients of A_0 in Equation 21 is
225 equivalently modified at the unit circle as

226 $$\Phi_0(\sigma)+\overline{\Phi_0(\sigma)}=\sum_{n=1}^{+\infty}A_{-2n}\frac{1}{\sigma^{2n}}+\frac{A_0}{2|\sigma|^2}+\frac{A_0}{2}|\sigma|^2+\sum_{n=1}^{+\infty}A_{2n}\sigma^{2n} \qquad (22)$$

227 By multiplying both sides with $\frac{1}{2\pi i}\frac{d\sigma}{\sigma-\zeta}$ (here ζ is a point within Ω^-) and then integrating it along
228 the circumference of γ, Equation 22 gives

229 $$\Phi_0(\zeta)=\frac{A_0}{2|\zeta|^2}+\sum_{n=1}^{+\infty}\frac{A_{-2n}}{\zeta^{2n}} \qquad (23)$$

230 Then the general form of $\Phi(\zeta)$ can be obtained by releasing the previous assumption in the process of
231 deriving $\Phi_0(\sigma)$. The resultant vectors still equal to zero ($X=Y=0$) because of the continuous

distribution of stresses along the elastic-plastic boundary. With the use of Equation 12 and 23, the first complex potential goes to

$$\Phi(\zeta) = \frac{P_\infty}{2} + \Phi_0(\zeta) \tag{24}$$

Then the complex potential $\Psi(\zeta)$ is derived by integrating the continuity condition of the deviatoric stress (i.e. Equation 11a) along γ from the side of Ω^- with the Cauchy integral method. As discussed in Appendix B, all terms in Equation 11a are holomorphic in Ω^-, therefore $\Psi(\zeta)$ goes to

$$\Psi(\zeta) = k\frac{(\beta\zeta^2+1)}{(\zeta^2+\beta)}\left\langle \frac{\sqrt{\hat{r}^4 - m^2R^4} + mR^2 i}{\hat{r}^2} \right\rangle - \frac{\zeta(\beta\zeta^2+1)}{\zeta^2-\beta}\Phi'(\zeta) \tag{25}$$

where $\hat{r}^2 = \alpha^2(1+\beta^2+\beta\zeta^2+\beta\zeta^{-2})$. $\Phi'(\zeta)$ is the derivative of the complex potential $\Phi(\zeta)$ with respect to ζ, which can be easily calculated with $|\zeta|^2 = \xi^2+\eta^2$ and $\frac{\partial}{\partial\zeta} = \frac{1}{2}(\frac{\partial}{\partial\xi} - i\frac{\partial}{\partial\eta})$. Hence,

$$\Phi'(\zeta) = -\frac{A_0}{2\zeta|\zeta|^2} - \sum_{n=1}^{+\infty} 2n\frac{A_{-2n}}{\zeta^{2n+1}} \tag{26}$$

Now this stress boundary value problem is analytically solved through the combination use of the Cauchy integral method and Fourier series as shown in Equations 23-26.

4 | DISCUSSION ON RESTRICTIONS FROM THE ASSUMPTIONS

As stated in Section 3.1, the above static stress solution was derived based on several prior assumptions. Restrictions due to these assumptions are discussed as follows.

(1) The cavity is fully enclosed by a plastic region

This assumption requires that the inner cavity is fully enclosed by a continued plastic region. Limit conditions of this requirement will be approached while the vertices of the predicted elastic-plastic boundary in the minor axis direction just reach the cavity wall [33]. It gives

$$b_{ep} = \alpha(1-|\beta|) \geq R \tag{27}$$

(2) Intermediate principal stress

It was assumed that the out-of-plane stress σ_{zz} always remains as the intermediate principal stress. Although this assumption is always justified for incompressible conditions, restrictions will be produced in compressible materials. The plastic stress solutions show that the principal stresses in the plastic zone vary from the inner cavity wall to the elastic-plastic boundary monotonically. Therefore, it just needs to ensure that values of σ_{zz} at the inner cavity wall and at the vertices on the major axis of the elastic-plastic boundary always remain as the intermediate principal stress [33]. Relationships between the principal stresses and other stress components are given in Appendix A. With the aid of Equations 7, 8, and 9, this restriction for compressible Tresca materials can be expressed as

$$\sqrt{1-m^2}-\frac{1}{1-2\nu}+\ln(\Theta)\le\frac{p_{in}}{k}\le\sqrt{1-m^2}+\frac{1}{1-2\nu} \tag{28}$$

where $\Theta=\dfrac{[\alpha(1+|\beta|)/R]^2+\sqrt{[\alpha(1+|\beta|)/R]^4-m^2}}{1+\sqrt{1-m^2}}>1$.

(3) Static determinacy of the plastic zone

The plastic stresses were derived by assuming that the plastic zone is statically determinate. Theoretically, it implies that every point in the plastic region can be connected to the cavity rim by two characteristic lines (slip-lines) of different families, and every slip-line cuts the elastic-plastic boundary only once [51]. Therefore, the limit condition will be reached while one, and only one, characteristic line is tangent to the elastic-plastic interface within one quadrant.

It is known that directions of the slip-lines take an angle of $\pi/4$ with the principal stress directions in Tresca materials. While internal shear stresses apply, the radial and circumferential directions are no longer the principal stress directions in the plastic zone. As shown in Figure 2, the direction of the minor principal stress takes an anticlockwise rotation to the radial direction of the cylindrical coordinates with positive shear stresses at the inner cavity wall. Contrarily, a clockwise rotation would be caused by negative shear stresses. Here taking the anticlockwise direction of φ as positive, according to Figure 3, the requirement of this assumption can be expressed as

$$|\lambda-\theta|\le\frac{\pi}{4}+\varphi \tag{29}$$

where θ is the angle between the radial direction and the x-axis. λ represents the angle between the outward normal to the elastic-plastic interface and the x-axis.

Angles in Equation 29 all can be expressed in terms of the unit complex variable σ as

$$e^{2i(\lambda-\theta)} = \sigma^2 \frac{\omega'(\sigma)}{\overline{\omega'(\sigma)}} \frac{\overline{\omega(\sigma)}}{\omega(\sigma)} = \frac{(\sigma^2-\beta)}{(1-\beta\sigma^2)} \frac{(1+\beta\sigma^2)}{(\beta+\sigma^2)} \quad ; \; 2\varphi = \arcsin\left[m \frac{R^2}{\omega(\sigma)\overline{\omega(\sigma)}} \right] \tag{30}$$

where $\omega(\sigma) = \alpha(\sigma + \beta\sigma^{-1})$; $\overline{\omega(\sigma)} = \alpha(\sigma^{-1} + \beta\sigma)$.

To ensure that only one characteristic line reaches the limit condition within one quadrant, it restricts that the equality condition holds only when the function $g(\sigma) = |\lambda - \theta| - \varphi$ reaches its extremum [35]. The extremum values of $g(\sigma)$ lie at the zero points of its first derivative. If no shear stress is applied, this restriction becomes $|\beta| \le (\sqrt{2} - 1)$ [33, 35].

With the defined boundary conditions, stress states developed around the inner cavity can be broadly categorized into three conditions [26, 33]: a) purely elastic state (i.e. zone A); b) the cavity is partially surrounded by plastic regions (e.g., zone B and zone E); and c) the cavity is fully enclosed by a plastic region (e.g. zone C and zone D). The stress field in a purely elastic state can be readily calculated with the solution given in Appendix A. The limit pressure that a plastic zone starts forming from the inner cavity wall under loading is useful in estimating the plastic initiation pressure of fracturing [14], and, therefore, it is also given in Equation 31.

$$(p_{in} + P_\infty) \ge k\sqrt{1-m^2} - 2|\tau_\infty| \tag{31}$$

In the other two stress states, distributions of the plastic regions are various, mainly depending on the material strength and boundary conditions [26, 33]. By using Equations 27-31, example boundaries of different stress states are shown in Figure 4 for illustration. As previously discussed, the present solution is dedicated to problems with boundary stresses belonging to Zone C.

Without the internal shear stresses, Figure 4 shows that Equations 27-31 give the same results as that given by Yarushina et al. [33] for the problem of Galin [30], and the distribution patterns of the plastic regions in Zones D and E refer to Yarushina et al. [33]. When additional shear stresses apply, the limits of different

stress states would change. In specific, Line 2 (representing the limit given by Equation 27) moves leftwards with increasing shear stresses. Line 3 (determined by Equation 29) represents the limit of static determinacy of the plastic region. It is a horizontal line with a constant value of $|\beta| \le (\sqrt{2}-1)$ in the case without internal shear stresses, but becomes curved due to the rotation of principal stresses caused by the internal shear stresses. Opposite rotations will be produced by the shear stresses with different applying directions. As a result, the bounds of this requirement distribute in opposite sides of the horizontal line of $|\beta| \le (\sqrt{2}-1)$, but they both gradually approach to $(\sqrt{2}-1)$ with an increasing value of $\left|P_\infty + p_{in}\right| / k$. Line 4 reflects the restriction specified by Equation 28. The additional shear stresses exert little impact on this restriction. Example lines calculated with $p_{in} = 0$ and $\nu = 0.4$ are shown in Figure 4. Line 4 moves rightwards (or leftwards) with an increasing (or decreasing) Poisson's ratio, and this restriction will be released in incompressible materials.

5 | SOLUTION VALIDATION AND DISCUSSION

Within the permissible stress states specified by Equations 27, 28, and 29, the above solution for static stress analysis under loading can be calculated with the following steps.

(a) determine the elastic-plastic boundary by using the mapping function given in Equation 13. Then the plastic stress field can be obtained from Equations 7, 8, and 9 directly. One-to-one corresponding relations between the physical plane and the phase plane can be established by using Equation 32;

$$x = r\cos\theta = \alpha(\rho + \frac{\beta}{\rho})\cos\phi \ , \ y = r\sin\theta = \alpha(\rho - \frac{\beta}{\rho})\sin\phi \tag{32}$$

(b) calculate the coefficients of the established Fourier series (e.g. Equation 23), which stay the same values in the whole elastic filed (setting $n = 5$ in Equation 23 in the following calculations). The elastic complex potentials given in Equations 24 and 25 can then be calculated. By substituting the complex potentials into Equations 33 and 34, stresses in the elastic region can be readily obtained by separating the real and imaginary parts.

$$\sigma_x^e + \sigma_y^e = 4\,\mathrm{Re}[\Phi(\zeta)] \tag{33}$$

$$\sigma_y^e - \sigma_x^e + 2i\tau_{xy}^e = 2[\frac{\overline{\omega(\zeta)}}{\omega'(\zeta)}\Phi'(\zeta) + \Psi(\zeta)] \quad (34)$$

5.1 | Comparison with Galin's solution and finite element method

The analytical solution is validated by comparing with Galin's [30] solution (i.e. the special case of zero internal shear stress) and the finite element method (FEM) as shown in Figures 5 and 6 respectively. The FEM simulations are implemented in Abaqus/Standard 6.12 using the same linear elastic-perfectly-plastic Tresca model as the above analytical solution. Biaxial far-field stresses are applied at the outer boundaries (100 times of the cavity radius away from the centre) of the plane-strain FEM model, and the same stress boundary conditions are applied at the inner cavity wall as depicted in Figure 1. An 8-node biquadratic plane-strain quadrilateral element is utilised for meshing.

It was introduced that Galin's [30] solution is a special case that without shear stresses on the inner cavity wall of the present solution. Although different methods to decomposing the stress continuity conditions have been adopted in these two solutions, Figure 5 demonstrated that the present solution can fully recover to Galin's [30] solution while taking m=0. When internal shear stresses apply, the analytical predictions are in good agreements with the FEM simulations as shown in Figure 6. It is found that the influence of the additional shear stress mainly concentrates in the plastic region, and the shear stress rapidly attenuates from the boundary value at the cavity wall to a stable level that varies in directions and depends on non-uniformity of the far-field stresses. Overall, it is shown that the developed series-form elastic complex potentials have good convergence precision and speed in computations, and the analytical solution can accurately calculate the surrounding elastic and plastic stress fields in the defined stress state.

5.2 | Distribution of elastic-plastic boundary

The range of the plastic zone developed around the inner cavity can be predicted by Equation 13. It is shown in Figure 7 that additional internal shear stresses extend the range of the plastic zone, but it imposes no influence on the shape of the elastic-plastic boundary (the major to minor axis ratio remains unchanged as $a_{ep} / b_{ep} = (1+|\beta|) / (1-|\beta|)$. The major axis of the elliptic elastic-plastic boundary under

loading lies in the x-axis direction while $\beta > 0$, whereas it is along the y-axis direction while $\beta < 0$. In other words, the direction of the major axis coincides with the direction of the minor principal stress (i.e. maximum compression stress) at infinity.

6 | QUASI-STATIC CAVITY EXPANSION SOLUTION IN A HYDROSTATIC STRESS FIELD

As previously discussed, rotations during cone penetrations may cause additional plastic failure in the surrounding soil comparing with non-rotated cone penetrations. It is believed that this effect contributes to the great reduction of the axial soil resistance measured by a rotating penetrometer [18, 19]. Based on the analogy of cone penetration and continuous cavity expansion, cylindrical cavity expansion solutions have been applied to estimate the normal soil pressure acting on non-rotated cones with some successes [39, 40]. In rotating CPTs, a rotating cone displaces the ahead soil increasingly cylindrical [18]. Therefore, a cylindrical quasi-static expansion analysis considering internal shear stresses is developed to account for the impact of the additional plastic deformation on the normal soil resistance measured in rotating CPTs as follows.

The quasi-static analysis of a cylindrical cavity models the lateral soil response caused by a vertically advancing cone. The confining in-situ soil stresses in a horizontal plane are assumed to be uniform. With uniform in-situ stresses, the mapping function of the elastoplastic interface (i.e. Equation 13) will reduce to $\omega(\sigma) = \alpha\sigma$. Therefore, the inner pressure during expansion can be expressed as

$$\frac{p_{in} + P_{\infty}^{h}}{k} = 2\ln\left(\frac{r_c^{h}}{\delta R}\right) + \sqrt{1 - m^2} \tag{35}$$

where r_c^{h} is the elastic-plastic radius under the corresponding hydrostatic initial stress of P_{∞}^{h}.

Radial displacements during continuous cavity expansions can be obtained by using the derived large-strain displacement solution in Appendix C. By letting $r = R$ and $r_0 = R_0$ in Equation C8, the radius ratio (r_c^{h} / R) of the elastic-plastic boundary to the current cavity at any expansion instant can be expressed as Equation 36.

374
$$\left[1-\frac{k}{2G}\sqrt{1-m^2\left(\frac{R}{r_c^h}\right)^4}\right]^2(\frac{r_c^h}{R})^2-(\frac{R_0}{R})^2 = \frac{1}{\varpi^2-1}\left[\left(\frac{(r_c^h/R)^2+\sqrt{(r_c^h/R)^4-m^2}}{1+\sqrt{1-m^2}}\right)^{\varpi}(1+\varpi\sqrt{1-m^2})-[(\frac{r_c^h}{R})^2+\varpi\sqrt{(\frac{r_c^h}{R})^4-m^2}]\right] \quad (36)$$

375 While regarding the material as incompressible (i.e. $v=0.5$), the displacement solution of Zhou et al.[13]
376 can be recovered by Equation 36 as:

377
$$\frac{r_c^h}{R}=\sqrt[4]{\left[\frac{G}{k}[(1-(\frac{R_0}{R})^2]\right]^2+m^2} \quad (37)$$

378 Equation 36 gives that a limit value of r_c^h/R exists during continuous expansions. This limit can be
379 approached by putting $R_0/R\to\infty$. In the special case of zero internal shear stress (i.e. $m=0$), the
380 limit ratio of r_c^h/R given by Yu [1] from a rigorous similarity analysis, considering the material
381 compressibility, can be recovered as given in Equation 38, neglecting the small quantities.

382
$$\frac{r_c^h}{R}=\left[(\varpi-1)(1-\frac{k}{2G})^2+1\right]^{\frac{1}{2(\varpi-1)}} \quad (38)$$

383 A rigorous quasi-static expansion solution is obtained by the combination use of Equations 35 and 36.
384 In the simplified cases of $v=0.5$ and $m=0$, the well-known limit expansion pressure derived by
385 Gibson and Anderson [54] (i.e. Equation 39) can be recovered by substituting the limit value of r_c^h/R
386 into Equation 35.

387
$$p_{limit}=k[1+\ln(\frac{G}{k})]-P_\infty^h \quad (39)$$

388 By using Equations 35 and 36, influences of the internal shear stress on the continuous pressure-
389 expansion response and the limit expansion pressure are depicted in Figures 8 and 9, respectively. It is
390 shown that additional shear stresses reduce the required normal pressure during continuous expansions,
391 and the limit expansion pressure declines with increases of the applied shear stresses and decreases of
392 Poisson's ratio. These reductions are due to the additional plastic failure caused by the internal shear
393 stresses. With fully mobilised shear stresses (i.e. m=1), a reduction of 6% of the limit expansion pressure

may be produced within the Tresca material, and this influence would be intensified in materials with greater interface shear stress holding capacity. In addition to the stress reorientation effect considered by Bengough, et al. [18], this solution provides an analytical method to further explain the great reduction of soil resistance measured in rotating CPTs.

7 | ESTIMATION OF MAXIMUM MUD PRESSURE IN HORIZONTAL DIRECTIONAL DRILLINGS

In the cavity expansion approach, the maximum mud pressure (p_m) in HDD practices is usually expressed in terms of the maximum allowable plastic radius (R_c). Based on the derived mapping function in Equation 13, p_m in terms of R_c can be expressed as

$$p_m = 2k\ln\left(\frac{R_c}{\delta R}\right) - P_\infty + k\sqrt{1-m^2} + u_0 \tag{40}$$

where u_0 is the groundwater pressure at the depth of the borehole.

According to Equations 13 and 35, the propagation distance of the plastic failure zone ($r_{c\theta}$) under biaxial stress conditions within the admissible stress range can be expressed as

$$r_{c\theta} = |\omega(\sigma)| = r_c^h \left|(\sigma + \frac{\beta}{\sigma})\right| \tag{41}$$

It has been demonstrated that the average cavity displacement in a biaxial stress field can be approximated by the solution derived in the corresponding hydrostatic stress condition [34, 55]. Therefore, the borehole radius pressurised under a uniform mud pressure is estimated by using the displacement solution given in Appendix C. With known initial borehole diameter ($2R_0 = D$) and radius of the elastic-plastic boundary, r_c^h / R can be obtained by letting $r = R$ and $r_0 = R_0$ in Equation C8 as:

$$(1-M)^2 - (\frac{R_0}{r_c^h})^2 = \frac{1}{\varpi^2 - 1}\left[\left(\frac{1+\sqrt{1-m^2(R/r_c^h)^4}}{[1+\sqrt{1-m^2}](R/r_c^h)^2}\right)^{\varpi}(1+\varpi\sqrt{1-m^2})(\frac{R}{r_c^h})^2 - [1+\varpi\sqrt{1-m^2(R/r_c^h)^4}]\right] \tag{42}$$

Neglecting the internal shear stress, r_c^h / R can be explicitly expressed as:

$$\frac{r_c^h}{R}=\left\{(\varpi-1)[(1-\frac{k}{2G})^2-(\frac{R_0}{r_c^h})^2]+1\right\}^{\frac{1}{2(\varpi-1)}} \quad \text{(special case of } m=0\text{)} \tag{43}$$

In undrained clays, the plastic volumetric change under loading is often negligible. Therefore, the displacement solution can be further simplified to the Delft solution in this case [56] as Equation 44.

$$\frac{r_c^h}{R}=\left[\frac{k}{G}+(\frac{R_0}{r_c^h})^2\right]^{-\frac{1}{2}} \quad \text{(special case of } m=0 \text{ and } \nu=0.5\text{)} \tag{44}$$

The failure model caused by pressurized drilling fluids in clays is considered to be either tensile or shear failure [57-59]. The limit failure pressure varies with the failure model significantly. In general, the tensile fracture pressure is lower than that with shear failure [17, 58]. The failure model primarily depends on the material strength and stress conditions (e.g. the K_0 effect) within homogenous materials [50, 60]. Both elastic (e.g. Kirsch equations) and elastic-plastic (e.g. Delft solution) cavity expansion solutions are often applied to estimate the limit pressure based on different failure criteria [5, 14, 17, 60]. Based on the cavity expansion analysis, the potential failure models under loading may refer to the discussion given in Section 4. Taking Figure 4 as an example, tensile fracture failure tends to occur within the stress ranges of Zones B and E; shear failure may dominate in the Zone C; and a mixed failure may take place in the Zone D. As discussed earlier, the present stress solution was derived under stress conditions within the Zone C. Therefore, Equations 40, 41, and 42 are preferable for estimating the maximum mud pressure of HDDs implemented under stress conditions within this stress range.

For horizontal boreholes excavated at relatively shallow depths, apart from the considered K_0 effect, the free ground surface and soil strength and stress gradient with depths may also influence the failure model. The cavity expansion solutions used for this application were mostly developed in an infinite plane. Therefore, different criteria have been proposed in the cavity expansion approach to estimating the maximum mud pressure during HDDs, for example, the maximum allowable plastic radius criterion [42, 61] and maximum hoop strain criterion [5]. Evaluation of the reliability of these criteria is out of the scope of this paper. Instead, the most commonly adopted maximum allowable plastic radius criterion is followed in this solution.

Comparing with the elastic-plastic radius calculated in the corresponding hydrostatic stress condition (Equation 42), a shape factor of $\left|\sigma+\beta/\sigma\right|$ is introduced by Equation 41 due to the biaxial in-situ stresses. It is shown in Figure 10 (a) that Equation 41 describes that the plastic zone develops farther in the vertical direction while $K_0<1$ (e.g. in normally consolidated or lightly overconsolidated clays), whereas the farthest yielding point is along the horizontal direction before failure while $K_0>1$ (e.g. heavily overconsolidated clays). Similar trends have also been reported in numerical and experimental studies [56, 62]. However, it needs to point out that the propagation of the plastic zone in cases of $K_0>1$ may rapidly extend to the free ground surface at the ultimate failure stage instead of propagating farther in the horizontal direction, and, consequently, caution should be exercised when the maximum allowable plastic radius criterion is applied in this case. Therefore, the following discussion concentrates on the performance of the present solution in cases of $K_0\le 1$.

Following the failure criterion suggested by the Delft solution, which states that the maximum allowable mud pressure will be reached when the plastic region expands to a distance equalling to half of the burial depth, the new method given by Equations 40-42 is applied to estimate p_m for cases while $K_0\le 1$. While $K_0\le 1$, the farthest yielding point locates above the crown of the borehole with a centre distance of $R_c=r_c^h\left(1-\beta\right)=0.5H$. Based on numerical simulation results, Xia and Moore [17] reported that the Delft solution may overestimate the mud pressure by up to 15% while $K_0<1$, and better agreements with the numerical results have been achieved by their solution considering the K_0 effect [56]. Figure 10 (b) demonstrated that the K_0 effect is also well captured by the present solution in the given stress states. Additionally, it is shown that internal shear stresses may lead to further decreases of the maximum allowable mud pressure. Hence, the ignorance of the internal shear stresses may be another noticeable reason that leads to that the Delft solution generally tends to overestimate p_m in practice [45, 47].

8 | SUMMARY AND CONCLUSIONS

An analytical elastoplastic stress solution was developed for a cylindrical cavity under loading in Tresca materials, subjected to biaxial stresses at infinity and uniform normal and shear stresses on the cavity wall. The solution was derived by three steps: a) plastic stresses were derived by assuming that the plastic zone is statically determinate, b) a conformal mapping function describing the outside elastic region was determined through analysing the stress continuity conditions across the elastic-plastic boundary based on Laurent's decomposition theorem and Harnack's theorem, and c) Kolosov-Muskhelishvili complex potentials for the elastic analysis were obtained by using the Cauchy integral method and Fourier series method. Within the admissible application range, the analytical solution showed excellent agreement with FEM simulations and Galin's solution in the special case without internal shear stresses. It was demonstrated that both the internal shear stress and biaxial in-situ soil stresses have fairly significant influences on the distribution of the plastic zone. It was shown that the elastic-plastic boundary is in an elliptic shape under biaxial stress conditions, whose major axis coincides with the direction of the maximum far-field compression stress under loading on the internal cavity wall. The additional shear stresses extend the plastic region, but apply no influence on the shape of the elastic-plastic boundary. In addition, considering the internal shear stresses, an analytical large strain displacement solution was developed for a cylindrical cavity expanding in a hydrostatic in-situ stress field. The derived stress and displacement solutions were applied to account for the additional influence of the shear stresses generated during rotating CPTs and to estimate the maximum allowable mud pressure of HDDs considering both biaxial in-situ stresses and the possibly generated internal shear stresses.

To explain the reduction of the normal soil resistance in rotating CPTs due to the shear stresses generated around the interface, an analytical quasi-static cavity expansion solution was developed by combing the derived static stress solution and the continuous displacement solution. It was found that the internal shear stresses would lead to additional plastic failure in the surrounding soil. As a result, the required normal pressure during expansions and the limit normal expansion pressure decline, depending on the shear stress level. These findings further explained the great reduction of the tip

resistance measured in rotating CPTs in addition to the reorientation effect of the interface frictional resistance.

Considering the K_0 effect and influences of the shear stresses generated during drillings, a new approximate method for estimating the maximum allowable mud pressure during HDDs was developed. With the same maximum allowable plastic radius as in the Delft solution, the new method predicted lower maximum mud pressures than those by the Delft solution in cases of $K_0 < 1$ and showed that the maximum mud pressure declines with a decreasing value of K_0. These findings are consistent with that reported in numerical simulations. In addition, it was found that the internal shear stresses may also cause a considerable reduction of the maximum mud pressure in HDDs, which suggested that this effect may need to be considered while a significant amount of shear stresses between the rotating drill bit/reamer and the surrounding soil are unavoidably generated during drillings.

Appendix A. Purely elastic stress solutions and expressions of principal stresses [1]

$$\sigma_r = P_\infty\left(1-\frac{R_0^2}{r^2}\right)-\tau_\infty\left(1+\frac{3R_0^4}{r^4}-\frac{4R_0^2}{r^2}\right)\cos 2\theta - p_{in}\frac{R_0^2}{r^2} \tag{A1}$$

$$\sigma_\theta = P_\infty\left(1+\frac{R_0^2}{r^2}\right)+\tau_\infty\left(1+\frac{3R_0^4}{r^4}\right)\cos 2\theta + p_{in}\frac{R_0^2}{r^2} \tag{A2}$$

$$\tau_{r\theta} = \tau_\infty\left(1-\frac{3R_0^4}{r^4}+\frac{2R_0^2}{r^2}\right)\sin 2\theta + mk\frac{R_0^2}{r^2} \tag{A3}$$

$$\sigma_1 = \frac{\sigma_r+\sigma_\theta}{2}+\left[\left(\frac{\sigma_r-\sigma_\theta}{2}\right)^2+\tau_{r\theta}^2\right]^{1/2} \tag{A4}$$

$$\sigma_1 = \frac{\sigma_r+\sigma_\theta}{2}-\left[\left(\frac{\sigma_r-\sigma_\theta}{2}\right)^2+\tau_{r\theta}^2\right]^{1/2} \tag{A5}$$

$$\sigma_2 = \nu(\sigma_1+\sigma_3) \tag{A6}$$

Appendix B. Re-derivation of the mapping function [37]

To transform the exterior of the elastic-plastic boundary in the physical plane onto the exterior region of the unit circle in the phase plane, a general form of conformal mapping function is introduced [63] as

$$\omega(\zeta) = \alpha'\zeta + \alpha_0' + \sum_{n=1}^{\infty}\frac{\alpha_n'}{\zeta^n} \tag{B1}$$

Due to the symmetry of the geometry and stress boundaries, the mapping function $\omega(\zeta)$ has the following features [35].

$$\omega(\zeta) = -\omega(-\zeta) \quad , \quad \omega(\zeta) = \overline{\omega(\bar{\zeta})} \tag{B2}$$

As a result, α_0 and coefficients of the even order terms are equal to zero, and remaining coefficients are real numbers. $\omega(\zeta)$ can be rewritten as

$$\mathrm{z} = \mathrm{x} + \mathrm{iy} = \omega(\zeta) = \alpha\zeta + \sum_{\mathrm{j}=0}^{\infty} \frac{\alpha_{2\,\mathrm{j}+1}}{\zeta^{2\,\mathrm{j}+1}} \tag{B3}$$

By multiplying both sides of Equation 11a with $\frac{1}{2\pi \mathrm{i}} \frac{\mathrm{d}\sigma}{\sigma - \zeta}$, a Cauchy integral is established as:

$$\frac{1}{2\pi \mathrm{i}} \int_{\gamma} \left[\frac{\bar{\omega}(\sigma^{-1})}{\omega(\sigma)} \Phi'(\sigma) + \Psi(\sigma) \right] \frac{\mathrm{d}\sigma}{\sigma - \zeta} = \frac{\mathrm{k}}{2\pi \mathrm{i}} \int_{\gamma} \left\langle \frac{\sqrt{[\omega(\sigma)\overline{\omega(\sigma)}]^2 - \mathrm{m}^2 \mathrm{R}_0^{\,4}} + \mathrm{m}\mathrm{R}_0^{\,2}\mathrm{i}}{\omega(\sigma)\overline{\omega(\sigma)}} \right\rangle \frac{\overline{\omega(\sigma)}}{\omega(\sigma)} \frac{\mathrm{d}\sigma}{\sigma - \zeta} \tag{B4}$$

The right part of Equation B4 should be bounded at infinity [27, 52], hence terms of $\mathrm{j} \geq 1$ in the mapping function vanish as shown in Equation B5.

$$\frac{\overline{\omega(\sigma)}}{\omega(\sigma)} = \frac{\bar{\omega}(\sigma^{-1})}{\omega(\sigma)} = \frac{\bar{\alpha}\sigma^{-1} + \bar{\alpha}_1\sigma + \bar{\alpha}_3\sigma^3 + \cdots}{\alpha\sigma + \alpha_1\sigma^{-1} + \alpha_3\sigma^{-3} + \cdots} = \frac{\bar{\alpha}_1}{\alpha} + \mathrm{M}(\sigma) \tag{B5}$$

where $\mathrm{M}(\sigma)$ is analytic on the exterior of contour γ, and $\mathrm{M}(\infty) = 0$. Similarly, we find

$$\frac{\bar{\omega}(\sigma^{-1})}{\omega(\sigma)} \Phi'(\sigma) = \mathrm{N}(\sigma) \tag{B6}$$

where $\mathrm{N}(\sigma)$ is analytic on the exterior of contour γ, and $\mathrm{N}(\infty) = 0$.

Meanwhile, $\Psi(\sigma)$ is holomorphic in Ω^- (including infinity points). Finally, according to Harnack's theorem [20], integrating Equation B4 along γ from Ω^+ side gives

$$\alpha_1 = \bar{\alpha}_1 = \frac{\tau_\infty}{\mathrm{k}} \alpha \tag{B7}$$

Therefore, the mapping function is in the form of Equation 13. Detailed knowledge about the complex variable methods in elasticity refers to the references of Muskhelishvili [20] and England [63].

Appendix C. Displacement solution for continuous expansions in a hydrostatic stress field

For a cavity deforms in a hydrostatic initial stress state, the radial displacement during continuous expansions can be obtained by a one-dimensional deformation analysis. Note that Zhou et al.[13] presented an analytical expansion solution for this problem by ideally regarding the material as volumetric incompressible. More generally, a new large-strain displacement solution considering the material compressibility is presented here. The elastic displacement is derived based on the small strain theory, and finite strain definitions are adopted in the plastic deformation analysis [64, 65].

During purely elastic expansions, the radial displacement (u_r) can be expressed as

$$u_r = r - r_0 = \frac{p_{in} + P_\infty^h}{2G}\left(\frac{R}{r}\right)^2 r \tag{C1}$$

According to the elastic stress solution (i.e. Equations A1, A2, and A3, ignoring the angle-dependent terms) and the yield criterion (i.e. Equation 5), it is found that a plastic zone starts forming from the inner cavity wall while $p_{in} \geq k\sqrt{1-m^2} - P_\infty^h$. While plastic zone appears, the radial displacement in the outside elastic zone can be obtained by replacing p_{in} with the compression pressure at the elastic-plastic boundary ($p_{r_c^h}$) and R with the radius of the elastic-plastic boundary (r_c^h) in the solution of Equation C1. $p_{r_c^h}$ can be calculated by substituting the elastic stress solution into the yield criterion as

$$p_{r_c^h} = k\sqrt{1-m^2\left(\frac{R}{r_c^h}\right)^4} - P_\infty^h \tag{C2}$$

Then the radial displacement at the elastic-plastic boundary is obtained based on the elastic solution as

$$u_r\big|_{r=r_c} = \frac{kr_c^h}{2G}\sqrt{1-m^2\left(\frac{R}{r_c^h}\right)^4} \tag{C3}$$

Due to the plastic volumetric strain rate is zero in Tresca materials, the compressibility equation in the plastic region [1] can be expressed as

$$\dot{\varepsilon}_r + \dot{\varepsilon}_\theta = \frac{1-2v}{2G}[\dot{\sigma}_r + \dot{\sigma}_\theta] \tag{C4}$$

With the initial stress boundary conditions, integrating Equation C4 gives

552 $$\varepsilon_r + \varepsilon_\theta = \frac{1-2v}{2G}[\sigma_r + \sigma_\theta - 2P_\infty^h] \quad \text{(C5)}$$

553 By adopting the definition of logarithmic strain to characterise the accumulative deformation, the radial
554 strain and circumferential strain respectively are

555 $$\varepsilon_r = \ln\frac{dr}{dr_0} \quad , \quad \varepsilon_\theta = \ln\frac{r}{r_0} \quad \text{(C6)}$$

556 By substituting the plastic stresses and Equation C6 into Equation C5, it gives

557 $$\ln[\frac{r}{r_0}\frac{dr}{dr_0}] = \varpi \ln\left[\frac{r^2 + \sqrt{r^4 - m^2R^4}}{(r_c^h)^2 + \sqrt{(r_c^h)^4 - m^2R^4}}\right] \quad (\text{with } \varpi = \frac{(1-2v)k}{G}) \quad \text{(C7)}$$

558 With the use of Equation C3, Equation C7 can be integrated over the interval [r, r_c^h], leading to

559 $$\left[1 - \frac{k}{2G}\sqrt{1 - m^2\left(\frac{R}{r_c^h}\right)^4}\right]^2 (r_c^h)^2 - r_0^2 = \frac{1}{\varpi^2 - 1}\left\{\left(\frac{(r_c^h)^2 + \sqrt{(r_c^h)^4 - m^2R^4}}{r^2 + \sqrt{r^4 - m^2R^4}}\right)^{\varpi}(r^2 + \varpi\sqrt{r^4 - m^2R^4}) - [(r_c^h)^2 + \varpi\sqrt{(r_c^h)^4 - m^2R^4}]\right\} \quad \text{(C8)}$$

560 Now the continuous radial expansion of a cylindrical cavity in a hydrostatic in-situ stress field can be
561 modelled by using Equation C8 without limitation of the deformation level.

562 ## ACKNOWLEDGEMENTS

563 The work included in this paper was partly conducted at the Nottingham Centre for Geomechanics
564 (NCG). The first author would like to acknowledge the financial supports provided by the University
565 of Nottingham and the China Scholarship Council for his PhD study.

566 ## REFERENCES

567 1. Yu HS. Cavity expansion methods in geomechanics. Dordrecht, the Netherlands: Kluwer Academic
568 Publishers; 2000.
569 2. Yu HS. The First James K. Mitchell Lecture: In situ soil testing: from mechanics to interpretation.
570 Geomechanics and Geoengineering: An International Journal. 2006;1 (3): 165-195.

571 3. Randolph MF, Dolwin R, Beck R. Design of driven piles in sand. Geotechnique. 1994;44 (3): 427-
572 448.
573 4. Yu HS, Mitchell JK. Analysis of cone resistance: review of methods. Journal of Geotechnical and
574 Geoenvironmental Engineering. 1998;124 (2): 140-149.
575 5. Keulen B. Maximum allowable pressures during horizontal directional drillings focused on sand.
576 Ph.D. Thesis. Delft, the Netherlands: Delft University of Technology; 2001.
577 6. Marshall AM. Tunnel-pile interaction analysis using cavity expansion methods. Journal of
578 Geotechnical and Geoenvironmental Engineering. 2012;138 (10): 1237-1246.
579 7. Mayne PW, Kulhawy FH. K0- OCR Relationships in Soil. Journal of the Soil Mechanics and
580 Foundations Division. 1982;108 (6): 851-872.
581 8. Mesri G, Hayat T. The coefficient of earth pressure at rest. Canadian Geotechnical Journal. 1993;30
582 (4): 647-666.
583 9. Mckenzie BM, Mullins CE, Tisdall JM, Bengough AG. Root–soil friction: quantification provides
584 evidence for measurable benefits for manipulation of root ‐ tip traits. Plant, Cell and Environment.
585 2013;36: 1085-1092.
586 10. Sadeghi A, Tonazzini A, Popova L, Mazzolai B. A novel growing device inspired by plant root soil
587 penetration behaviors. PloS one. 2014;9 (2): e90139.
588 11. Whalley WR, Leeds-Harrison PB, Clark LJ, Gowing DJG. Use of effective stress to predict the
589 penetrometer resistance of unsaturated agricultural soils. Soil and Tillage Research. 2005;84 (1): 18-
590 27. 10.1016/j.still.2004.08.003.
591 12. Waldron LJ, Constantin GK. Soil resistance to a slowly moving penetrometer. Soil Science.
592 1970;109 (4): 221-226.
593 13. Zhou H, Liu H, Kong G. Influence of shear stress on cylindrical cavity expansion in undrained
594 elastic–perfectly plastic soil. Géotechnique Letters. 2014;4 (3): 203-210.
595 14. Yanagisawa E, Panah AK. Two dimensional study of hydraulic fracturing criteria in cohesive soils.
596 Soils and Foundations. 1994;34 (1): 1-9.

15. Detournay E, John CMS. Design charts for a deep circular tunnel under non-uniform loading. Rock Mechanics and Rock Engineering. 1988;21 (2): 119-137.

16. Rao P, Cui J, Li J. Elastoplastic Solutions of Cylindrical Cavity Expansion Considering the K0 ≠ 1. In Geotechnical Special Publication: Advances in Soil Dynamics and Foundation Engineering, ASCE: Shanghai, China 2014; pp 433-443.

17. Xia HW, Moore ID. Estimation of maximum mud pressure in purely cohesive material during directional drilling. Geomechanics and Geoengineering: An International Journal. 2006;1 (1): 3-11.

18. Bengough AG, Mullins CE, Wilson G. Estimating soil frictional resistance to metal probes and its relevance to the penetration of soil by roots. European Journal of Soil Science. 1997;48 (4): 603-612.

19. Bishop RF, Hill R, Mott NF. The theory of indentation and hardness tests. The proceedings of the Physical Society. 1945;57 (3): 147–159.

20. Muskhelishvili NI. Some basic problems of the mathematical theory of elasticity. 4th ed.; Groningen, the Netherlands.: P. Noordhoff; 1963.

21. Stevenson AC. Complex potentials in two-dimensional elasticity. Proceedings of the Royal Society of London. Series A. Mathematical and Physical Sciences. 1945;184 (997): 129-179.

22. Kuznetsov VV. Stress concentration near an elliptical hole in an elastic-plastic plate. International Applied Mechanics. 1972;8 (5): 531-536.

23. Ivlev DD. On the determination of displacements in the Galin problem. Journal of Applied Mathematics and Mechanics. 1959;23 (5): 1414-1416.

24. Kerchman VI, Erlikhman FM. A variational method of solving an elastic-plastic problem for a body with a circular hole. Journal of Applied Mathematics and Mechanics. 1988;52 (1): 105-110.

25. Huang WC. Theoretical study of stress concentrations at circular holes and inclusions in strain hardening materials. International Journal of Solids and Structures. 1972;8 (2): 149-192.

26. Bradford IDR, Durban D. Stress and deformation fields around a cylindrical cavity embedded in a pressure-sensitive elastoplastic medium. Journal of Applied Mechanics. 1998;65 (2): 374-379.

27. Savin GN. Stress distribution around holes. Washington, D.C.: National Aeronautics and Space Administration; 1970.

624 28. Gao XL, Wei XX, Wang ZK. A general analytical solution of a strain-hardening elasto-plastic plate
625 containing a circular hole subjected to biaxial loading-with applications in pressure vessels.
626 International Journal of Pressure Vessels and Piping. 1991;47 (1): 35-55.
627 29. Lee YS, Gong H. Application of complex variables and pseudo-stress function to power-law
628 materials and stress analysis of single rigid inclusion in power-law materials subjected to simple tension
629 and pure shear. International Journal of Mechanical Sciences. 1987;29 (10): 669-694.
630 30. Galin LA. Plane elastic-plastic problem: plastic regions around circular holes in plates and beams.
631 Prikladnaia Matematika i Mekhanika. 1946;10: 365-386.
632 31. Ochensberger W, Celigoj CC, Ulz MH. Amendment to the Galin plane elastoplastic solution.
633 Journal of Engineering Mechanics. 2013;139 (11): 1658-1662.
634 32. Tokar G. Generalization of Galin's problem to frictional materials and discontinuous stress fields.
635 International Journal of Solids and Structures. 1990;26 (2): 129-147.
636 33. Yarushina VM, Dabrowski M, Podladchikov YY. An analytical benchmark with combined pressure
637 and shear loading for elastoplastic numerical models. Geochemistry, Geophysics, Geosystems. 2010;11
638 (8): 1-16. doi:10.1029/2010GC003130.
639 34. Zhou H, Kong G, Liu H. A semi-analytical solution for cylindrical cavity expansion in elastic–
640 perfectly plastic soil under biaxial in situ stress field. Geotechnique. 2016;66 (7): 584-595.
641 35. Detournay E. An approximate statical solution of the elastoplastic interface for the problem of Galin
642 with a cohesive-frictional material. International Journal of Solids and Structures. 1986;22 (12): 1435-
643 1454.
644 36. Cherepanov GP. On a method of solving the elasto-plastic problem. Journal of Applied Mathematics
645 and Mechanics. 1963;27 (3): 644-655.
646 37. Parasyuk OS. An elastic-plastic problem with a non-biharmonic plastic state. Prikladnaya
647 Matematika i Mekhanika. 1948;13: 367-370.
648 38. Zhuang PZ, Yu HS. A unified analytical solution for elastic-plastic stress analysis of a cylindrical
649 cavity in Mohr-Coulomb materials under biaxial in-situ stresses. Geotechnique. 2018.
650 doi.org/10.1680/jgeot.17.P.281.

651 39. Salgado R, Prezzi M. Computation of cavity expansion pressure and penetration resistance in sands.
652 International Journal of Geomechanics. 2007;7 (4): 251-265.
653 40. Salgado R, Mitchell JK, Jamiolkowski M. Cavity expansion and penetration resistance in sand.
654 Journal of Geotechnical and Geoenvironmental Engineering. 1997;123 (4): 344-354.
655 41. Knight M, Duyvestyn G, Gelinas M. Excavation of surface installed pipeline. Journal of
656 infrastructure systems. 2001;7 (3): 123-129.
657 42. Staheli K, Bennett D, O'Donnell HW, Hurley TJ. Installation of pipeline beneath levees using
658 horizontal directional drilling; Technical Report CPAR-GL-98-1. US Army Corps of Engineers:
659 Vicksburg, MS, USA, 1998.
660 43. Adedapo AA. Pavement deterioration and PE pipe behaviour resulting from open-cut and HDD
661 pipeline installation techniques. Ph.D. Thesis. Waterloo, Ontario, Canada: University of Waterloo;
662 2007.
663 44. Bennett D, Wallin K. Step by Step Evaluation of Hydrofracture Risks for HDD Projects. In
664 International Pipelines Conference 2008, Atlanta, GA, 2008.
665 45. Staheli K, Christopher G, Wetter L. Effectiveness of hydrofracture prediction for hdd design. North
666 American Society for Trenchless Technology (NASTT), Chicago, IL. 2010: (F-1-01) 1-10.
667 46. Baumert ME, Allouche EN, Moore ID. Experimental investigation of pull loads and borehole
668 pressures during horizontal directional drilling installations. Canadian geotechnical journal. 2004;41
669 (4): 672-685.
670 47. Rostami A, Yi Y, Bayat A. Estimation of Maximum Annular Pressure during HDD in Noncohesive
671 Soils. International Journal of Geomechanics. 2016;17 (4): 06016029.
672 48. Luger H, Hergarden H. Directional drilling in soft soil: Influence of mud pressures. In Proceedings
673 of the 3rd International Conference on Trenchless Technology-'No Dig 88', Washington D.C., United
674 States, 1988.
675 49. Vesic AS. Expansion of cavities in infinite soil mass. Journal of Soil Mechanics and Foundations
676 Division. 1972;98 (SM3): 265-290.

677 50. Kennedy M, Skinner G, Moore I. Limiting drilling slurry pressures to control hydraulic fracturing
678 during HDD through purely cohesive soil. In 57th Canadian Geotechnical Conference (GeoQuebec
679 2004), Quebec, Canada, 2004; pp 37-44.
680 51. Hill R. The mathematical theory of plasticity. London: Oxford University Press; 1950.
681 52. Chakrabarty J. Theory of plasticity (3rd Ed.). Oxford, UK.: Elsevier Butterworth-Heinemann; 2006.
682 53. Gamelin TW. Complex analysis. New York: Springer; 2001.
683 54. Gibson RE, Anderson WF. In situ measurement of soil properties with the pressuremeter. Civil
684 Engineering and Public Works Review. 1961;56 (658): 615-618.
685 55. Detournay E, Fairhurst C. Two-dimensional elastoplastic analysis of a long, cylindrical cavity under
686 non-hydrostatic loading. International Journal of Rock Mechanics and Mining Sciences &
687 Geomechanics Abstracts. 1987;24 (4): 197-211.
688 56. Xia HW. Investigation of maximum mud pressure within sand and clay during horizontal directional
689 drilling. Ph.D. Thesis. Kingston, Ontario, Canada: Queen's University; 2009.
690 57. Marchi M, Gottardi G, Soga K. Fracturing pressure in clay. Journal of Geotechnical and
691 Geoenvironmental Engineering. 2013;140 (2): 04013008.
692 58. Alfaro MC, Wong RC. Laboratory studies on fracturing of low-permeability soils. Canadian
693 Geotechnical Journal. 2001;38 (2): 303-315.
694 59. Lan H, Moore ID. Practical criteria for assessment of horizontal borehole instability in saturated
695 clay. Tunnelling and Underground Space Technology. 2018;75 (1): 21-35.
696 60. Guo J, He S, Deng Y, Zhao Z. New stress and initiation model of hydraulic fracturing based on
697 nonlinear constitutive equation. Journal of Natural Gas Science and Engineering. 2015;27: 666-675.
698 61. Latorre CA, Wakeley LD, Conroy PJ. Guidelines for installation of utilities beneath corps of
699 engineers levees using horizontal directional drilling; US Army Corps of Engineers, Engineer Research
700 and Development Center: Washington, DC, 2002.
701 62. Yan X, Ma B, Zeng C, Liu Y. Analysis of formation fracturing for the Maxi-HDD Qin River
702 crossing project in China. Tunnelling and Underground Space Technology. 2016;53: 1-12.
703 63. England AH. Complex variable methods in elasticity. Mineola, New York: Dover Publications, Inc;
704 2003.

64. Chadwick P. The quasi-static expansion of a spherical cavity in metals and ideal soils. The Quarterly Journal of Mechanics and Applied Mathematics. 1959;12 (1): 52-71.

65. Yu HS, Houlsby GT. Finite cavity expansion in dilatant soils: loading analysis. Geotechnique. 1991;41 (2): 173-183.

710 **Figures:**

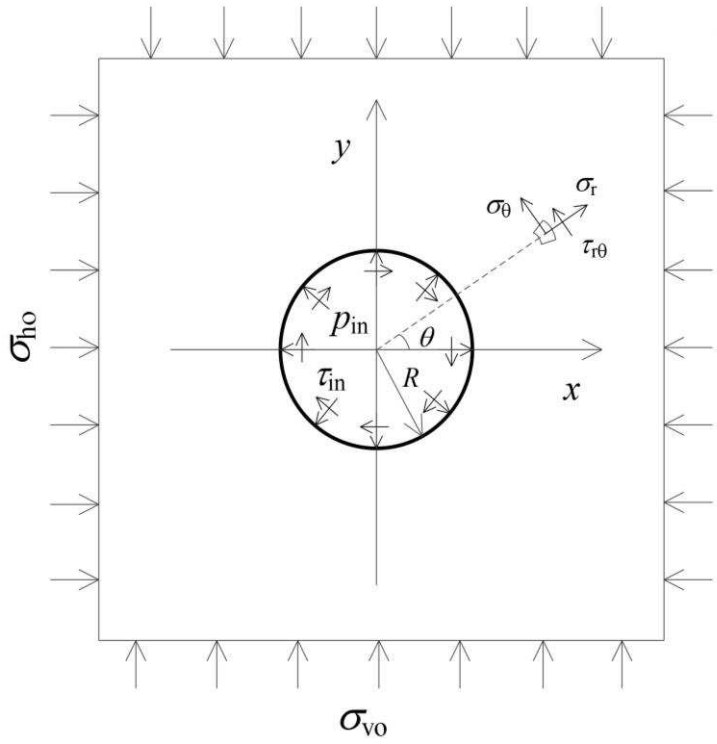

711

712 Figure 1 Stress boundaries and coordinate systems

713

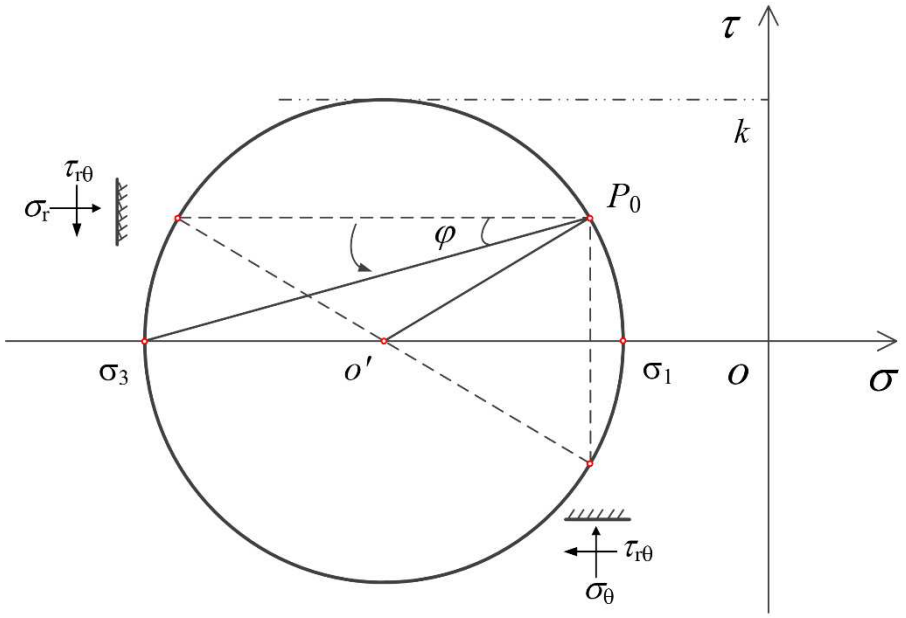

714

715 Figure 2 Direction of principal stresses

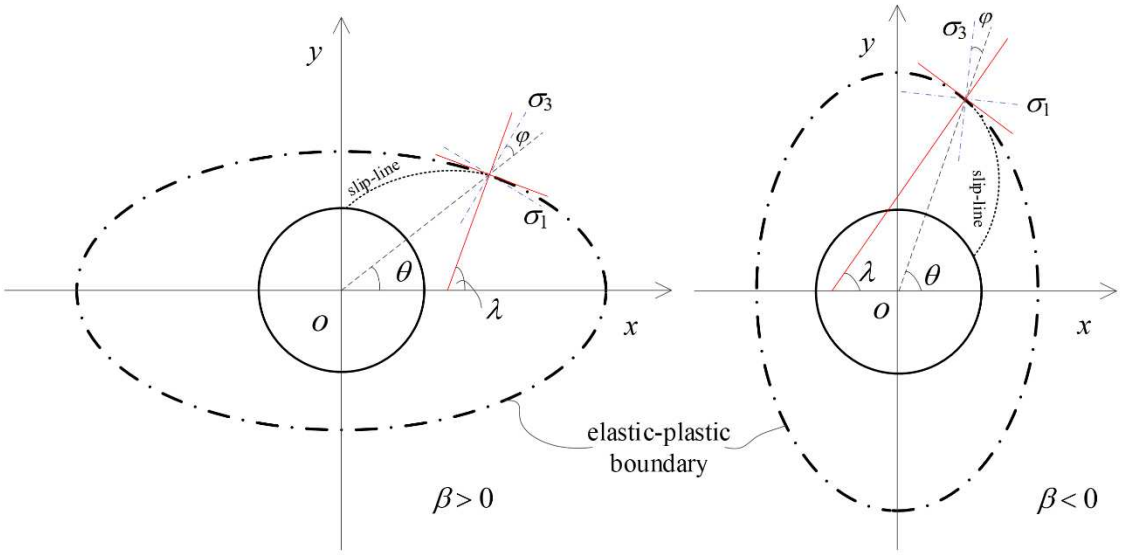

716

717 Figure 3 Illustration of slip lines intersecting with the elastic-plastic boundary (taking m>0 as an

718 example)

719

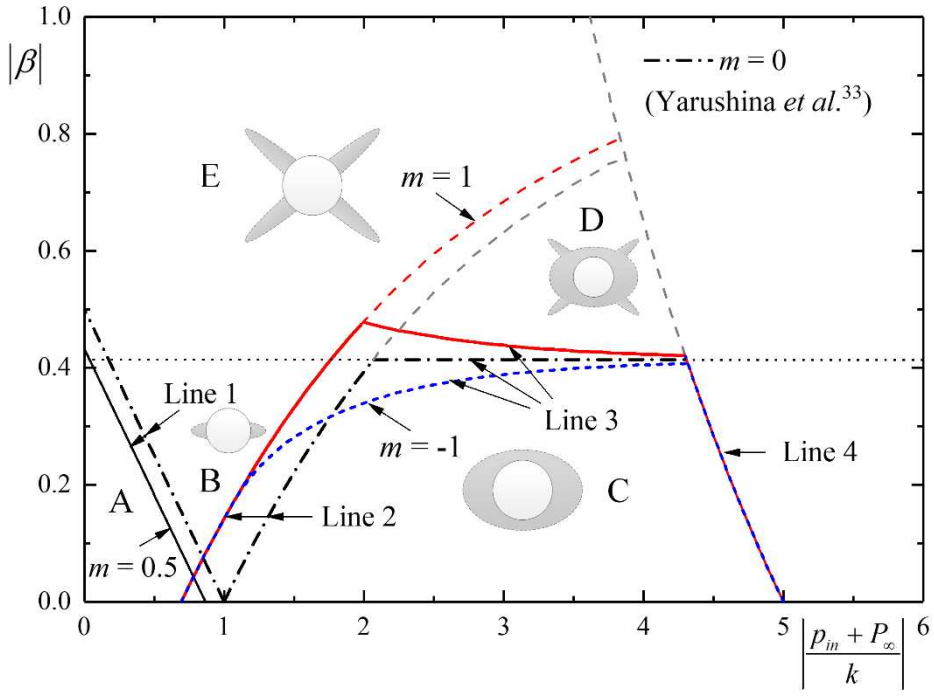

720

721 Figure 4 Example limits of different stress states ($\nu = 0.4$)

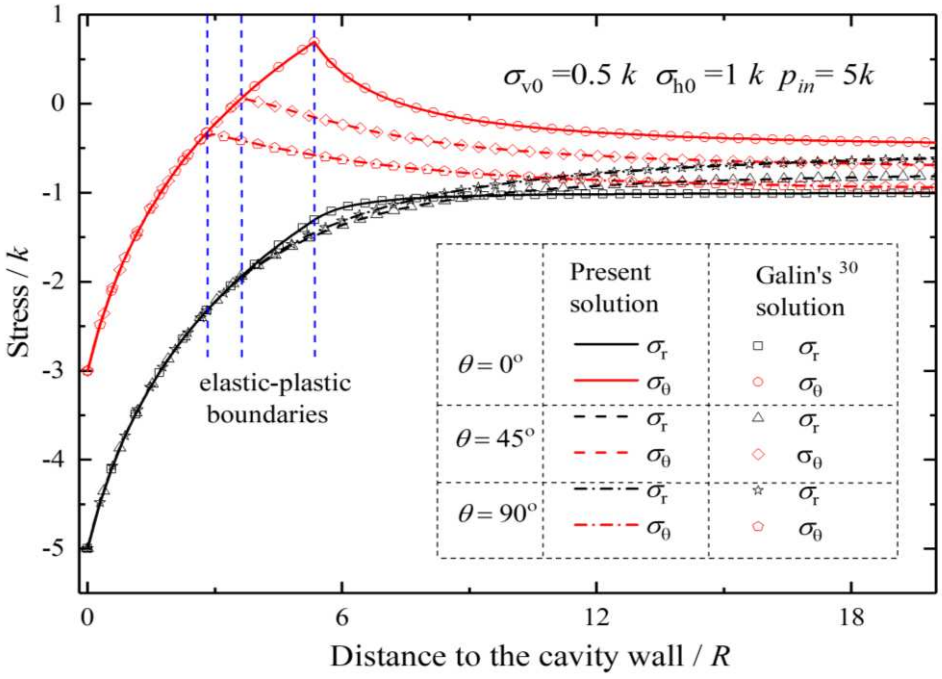

722

723 Figure 5 Comparison between the present solution with m=0 and Galin's [30] solution

724

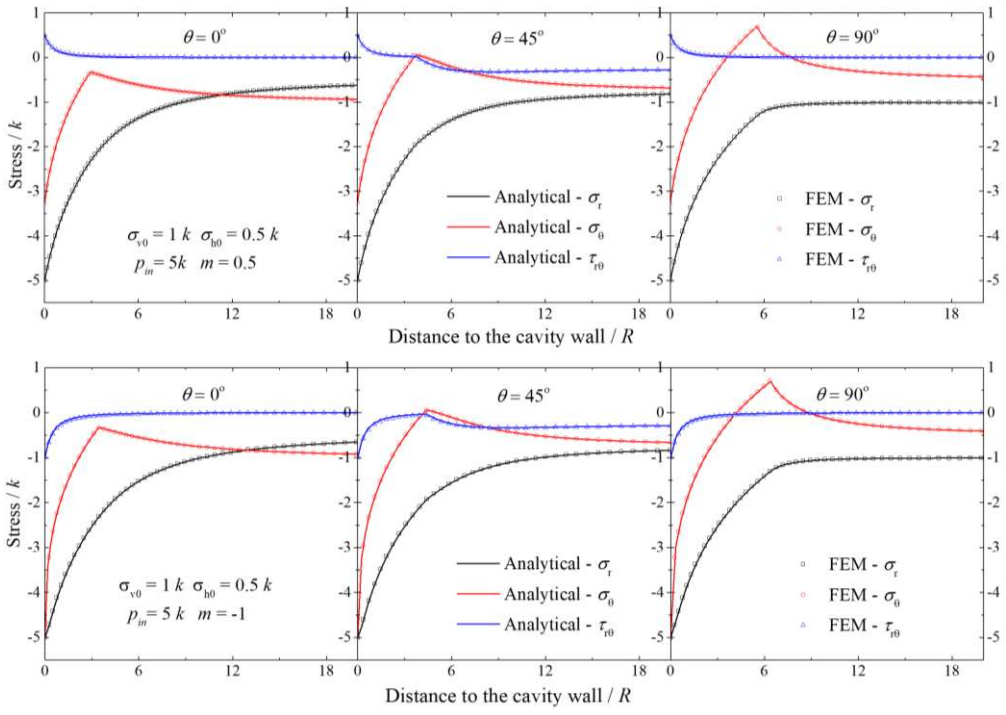

725

726 Figure 6 Comparison of stress components between the analytical solution and FEM simulations

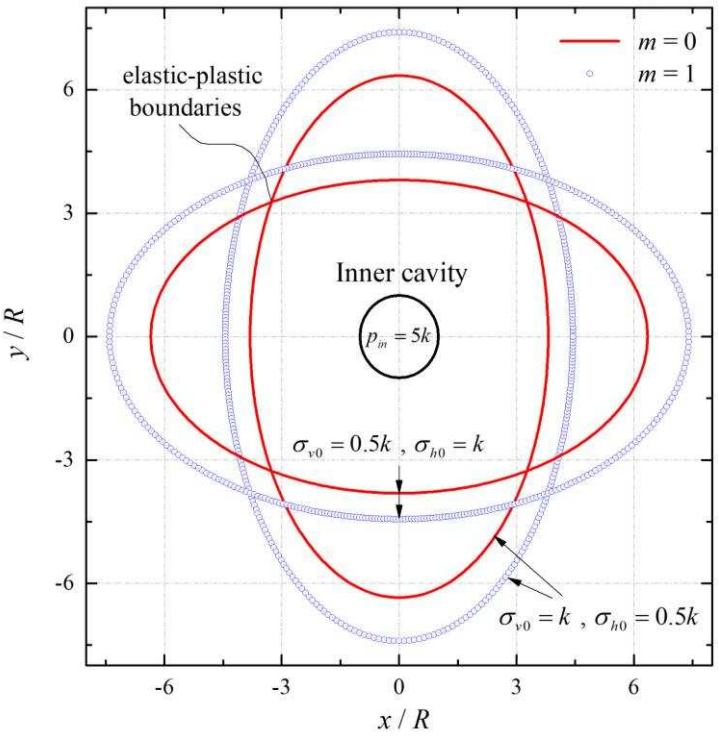

727

728 Figure 7 Influences of the internal shear stress and biaxial in-situ stresses on the elastic-plastic

729 boundary

730

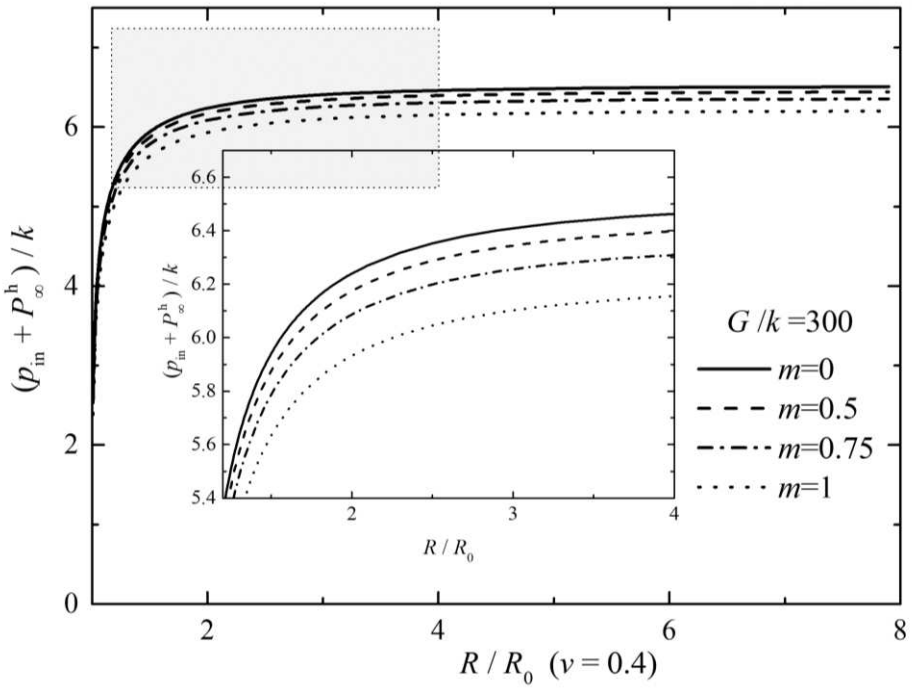

731

732 Figure 8 Example continuous pressure-expansion curves

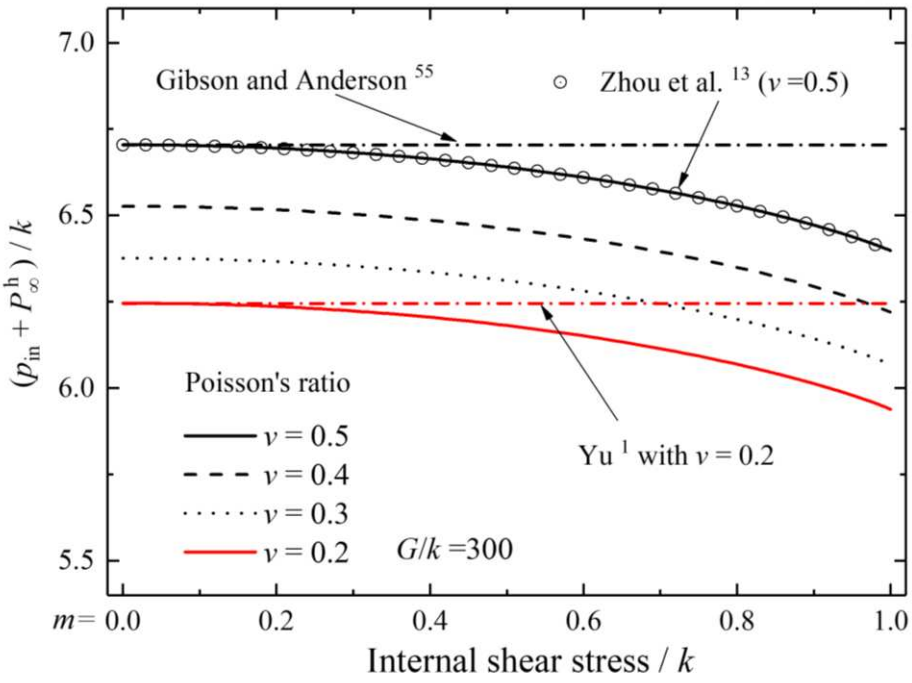

733

734 Figure 9 Influences of the internal shear stress on the limit expansion pressure

735

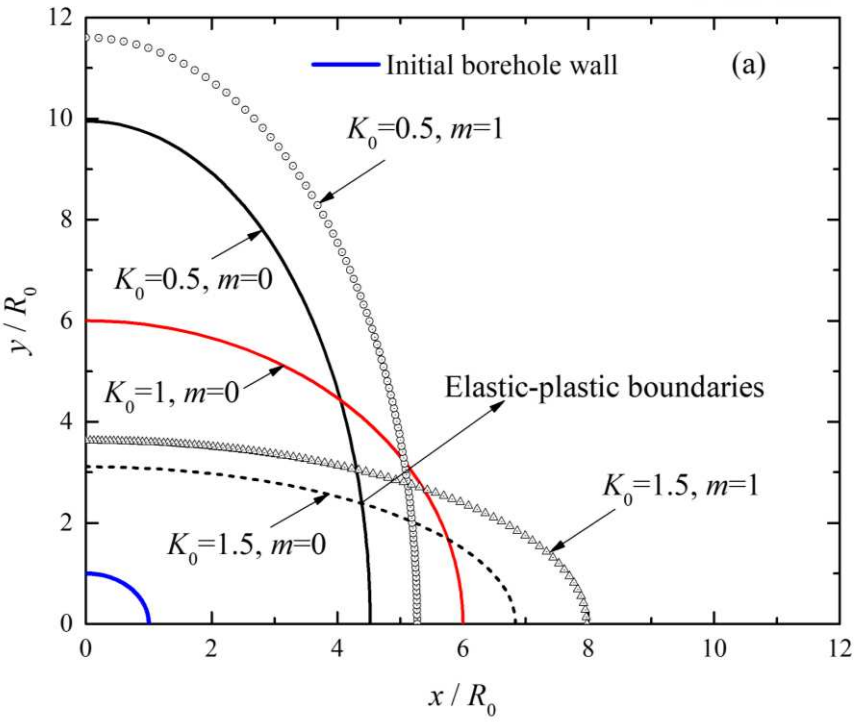

736

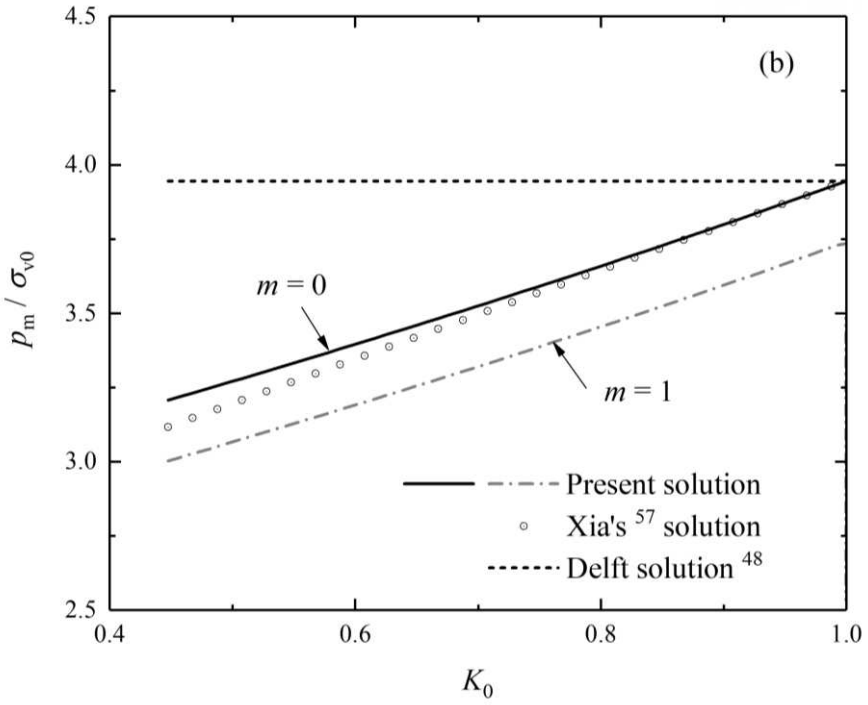

737

738 Figure 10 K_0 effect: (a) elastic-plastic boundaries with the same mud pressure; (b) limit mud pressures

739 with the same value of R_c(=0.5H) (H=3m, D=0.5m, G/k=200, v=0.5, k =40kPa, γ= 20 kN/m^3)